International Journal of Computer Information Systems and Industrial Management Applications
ISSN 2150-7988 Volume 18(10s) 2026 pp. 1192-1203
https://doi.org/10.70917/ijcisim-2026-3708
Article

Millimeter-Wave and THz Integrated Sensing and Communication Systems: Architecture and Applications in Smart Cities and V2X

B Nazeer Hussain[1], K Gopi[2]
[1]Assistant Professor,Vijayam Institute of Technology, Research Scholar, JNTU Ananthapur-515002.
nazeerhussain133@gmail.com
[2]Principal and Professor, Vijayam Institute of Technology, Chittoor - 517002
gopi.vijayamit@gmail.com

Abstract: Multi-band vehicle-to-everything integrated sensing and communication (ISAC) creates a decision conflict because the band that maximizes a direct communication link need not provide a reliable target echo. This paper proposes DSA-HISAC, a risk-aware heuristic for assigning a roadside unit and either 28 GHz or 142 GHz using conservative communication- and sensing-SNR estimates, predicted blockage, service risk, anticipated shared bandwidth, and frequency-band switching hysteresis. The method is evaluated at a four-way urban intersection with SUMO-generated motorized traffic and stochastic pedestrian crossings. The 28 GHz propagation model is 3GPP urban-microcell inspired, whereas 142 GHz uses measurement-derived outdoor exponents; both are simulation abstractions rather than claims of standards compliance. The revised campaign contains 120 matched runs across four traffic-demand levels and compares 13 methods, including joint-feasible, robust, and load-aware maximum-rate baselines. The primary equal-denominator metric assigns zero goodput when no link is selected or when either mandatory communication or sensing feasibility fails. DSA-HISAC attains a joint-feasibility fraction of 0.9467 and mean unconditional goodput of 2151.8 Mbit/s. Relative to load-aware robust max-rate, its changes are +1.19 percentage points in joint feasibility and +657.7 Mbit/s in unconditional goodput; the violation fraction among attempted selections changes from 1.283% to 0.022%. Compared with communication-only maximum-rate selection, DSA-HISAC changes joint feasibility by +12.94 percentage points and goodput by +899.5 Mbit/s. Risk-adaptive sensing reduces scheduled scan demand by 20.4% relative to fixed 10 Hz sensing, while information age is reset only after a valid sensing update. The results establish a controllable feasibility-goodput-overhead trade-off. They do not demonstrate end-to-end latency, packet reliability, beam tracking, standards compliance, or field safety.

Keywords: integrated sensing and communication, V2X, mmWave, sub-THz, dual SNR, blockage prediction, SUMO, unconditional goodput

1. INTRODUCTION

Roadside ISAC is attractive for connected and automated mobility because a common radio infrastructure can exchange V2X data while observing vehicles, pedestrians, cyclists, and occluded road users. Wide bandwidth and large arrays at millimeter-wave and sub-terahertz frequencies can improve both data rate and sensing resolution, but they also produce short-range coverage, blockage sensitivity, and frequency-dependent target scattering. A single communication-SNR or rate criterion therefore cannot represent a safety-relevant joint service.

The central problem considered here is deliberately narrower than a city-scale architecture problem. At each evaluation frame, a connected host is paired with its single highest-priority target within 60 m. The controller must select a roadside unit and one of two bands while accounting for direct-link quality, echo-link quality, predicted obstruction, expected sharing load, and switching cost. The output is evaluated as joint feasibility and goodput, not as certified road safety.

ETSI and 5GAA reports motivate road-intersection sensing cycles, detection requirements, and representative automotive service parameters. The ETSI city-zone intersection example specifies approximately a 60 m sensing range, horizontal resolution below 1 m, a 100 ms sensing cycle, false-positive probability below 0.1%, and false-negative probability below 0.01% [16]. The simplified detector and packet model used here do not reproduce those complete requirements. Likewise, the 5GAA values around a 300-byte message, 20 ms latency, and 99.9% reliability describe representative automotive service settings rather than universal ISAC requirements [17]. Accordingly, all thresholds in this paper are standards-informed exploratory inputs rather than evidence of compliance.

The paper makes four contributions:

• A dual-SNR selection formulation that separates direct communication quality from frequency-dependent target-echo quality.

• A conservative, load-aware heuristic that screens candidates, ranks feasible 28/142-GHz links, iterates expected bandwidth sharing, and applies band-switching hysteresis.

• A corrected equal-denominator evaluation using unconditional joint-service goodput, conditional successful-service rate, explicit no-selection probability, and joint-requirement violation fraction.

• A reproducible 120-run SUMO campaign with stronger joint-feasible baselines, ablations, valid-update information-age analysis, statistical tests, and parameter sensitivity.

2. Related Work and Research Gap

Foundational joint radar-communication and ISAC work established shared waveforms, beampattern design, information-theoretic trade-offs, and dual-functional wireless networks [1]–[3]. Vehicular studies subsequently exploited sensing for predictive beamforming, Bayesian motion estimation, learning-based beam prediction, complex-road tracking, and extended-target models [4]–[8]. These works directly address mobility and beam alignment; the present paper therefore does not claim a new beam-tracking algorithm.

At higher frequencies, sub-THz ISAC research emphasizes wideband propagation, hardware impairments, near-field effects, and measurement-backed channel modelling [9]–[12]. A 28 GHz connected-vehicle prototype has also demonstrated the feasibility of combining high-rate communication and radar-like ranging in controlled conditions [13]. These results support the relevance of high-frequency ISAC but do not by themselves resolve cross-band service selection under a weak or frequency-selective target echo.

Multi-band ISAC is now an active research topic. Recent work studies frequency diversity, multi-band detection, and resource allocation, including a July 2026 preprint on joint power and time-frequency allocation [14]. The novelty claim in this paper is therefore intentionally narrow: limited prior work jointly evaluates conservative direct-link and echo-link screening, predicted dynamic blockage, anticipated shared-bandwidth load, frequency-band hysteresis, and risk-adaptive sensing in a SUMO-based 28/142-GHz V2X intersection.

The closest conceptual baselines are joint-feasible maximum-rate selection and robust maximum-rate selection. These are included explicitly. DSA-HISAC is not presented as the solution of a general mixed-integer program; it is a structured heuristic that trades feasible service availability, unconditional goodput, sensing demand, and switching.

3. System and Signal Model

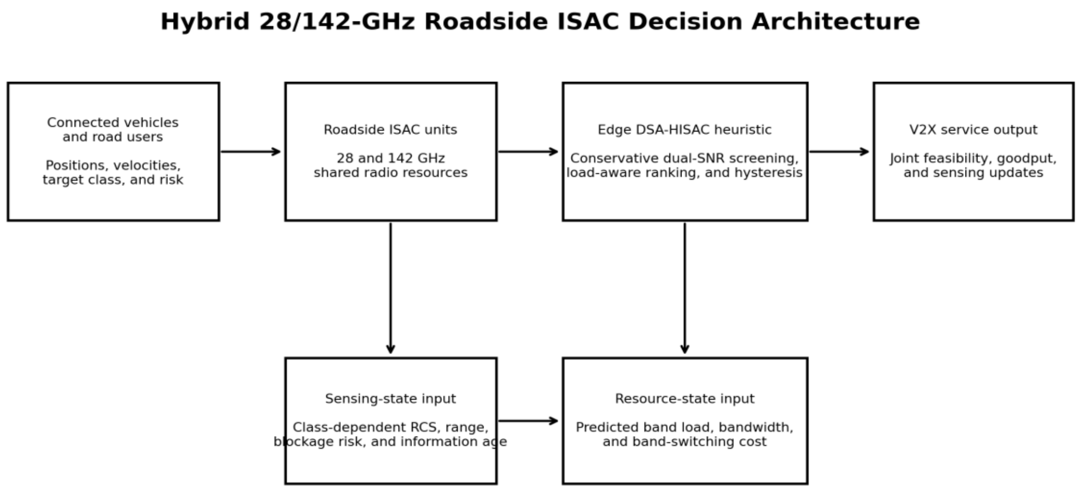

Fig. 1. Revised DSA-HISAC architecture. The controller ranks links using conservative dual-SNR estimates, predicted blockage, anticipated load, and hysteresis; no beam-tracking or certified latency function is claimed.

3.1 Urban-intersection scenario

Four roadside ISAC units are placed at the corners of a signal-controlled four-way intersection. Motorized mobility is generated by SUMO, and pedestrian crossings are added through a seeded stochastic process. Traffic inputs are reported as arrival demand in vehicles/hour/approach, not as physical density. Each connected host is associated with only its highest-risk target within 60 m for that frame. This keeps the decision problem reproducible but means that joint feasibility does not imply simultaneous protection of every nearby road user.

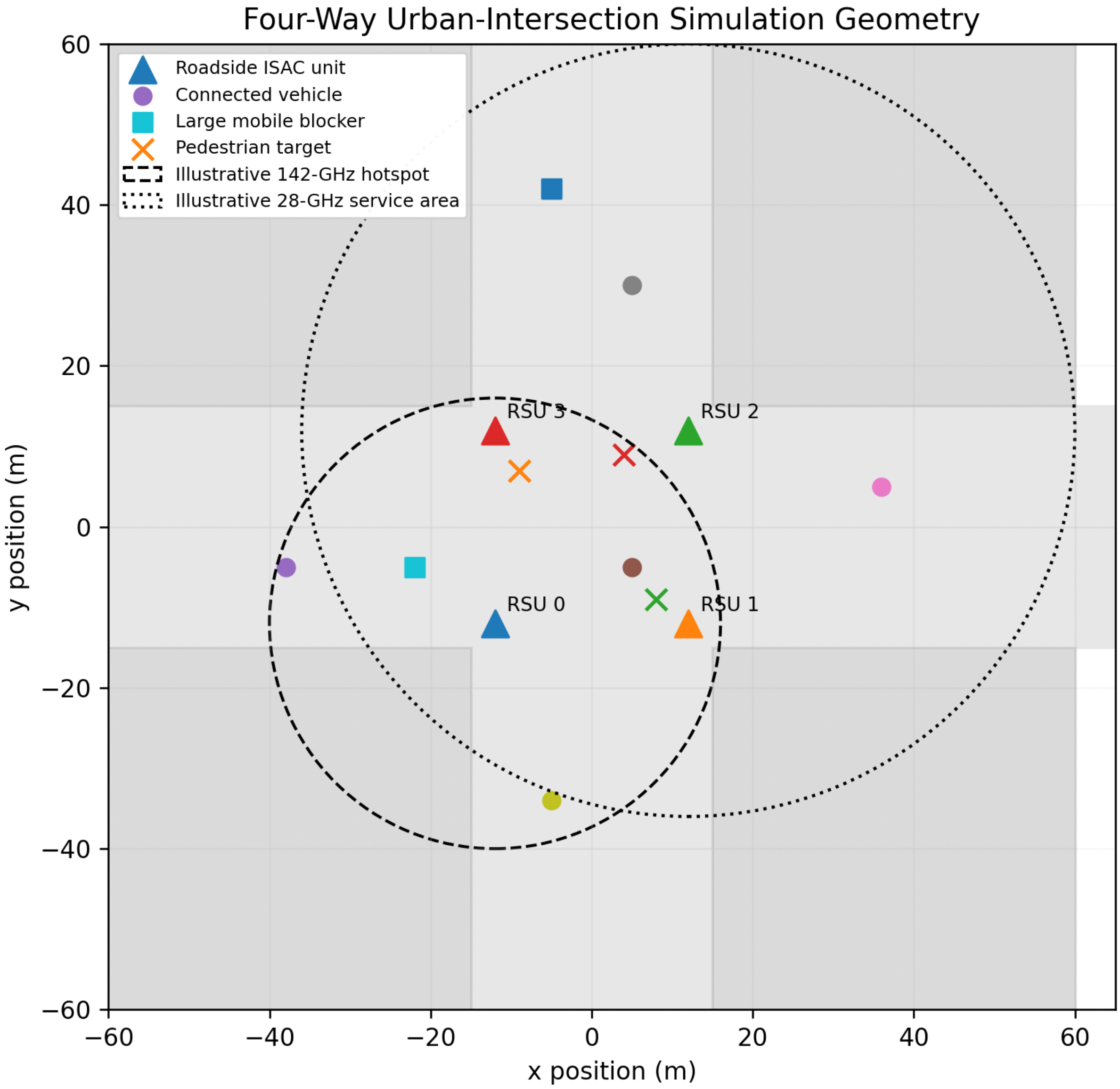

Fig. 2. Simulated urban intersection. Coverage circles are illustrative; propagation and blockage are computed for each RSU-object link.

3.2 Communication link

For roadside unit m, host k, band b, and frame t, the direct-link SNR is

$$\gamma^{c}_{mk\beta}(t) = P_{m\beta}\, G^{t}_{m\beta}\, G^{r}_{k\beta} \,/\, [(I_{mk\beta} + N_0 B_\beta) L_{mk\beta}(t)] \qquad (1)$$

where L includes frequency-dependent path loss, atmospheric attenuation, shadowing, building obstruction, and dynamic vehicle blockage. The 28 GHz model uses the urban-microcell structure of 3GPP TR 38.901 within its stated frequency scope; 142 GHz uses outdoor measurement-derived exponents. The implementation should be read as 3GPP-inspired at 28 GHz, because the complete geometry and all calibration conditions do not reproduce a specific standard test case.

When n users share the same RSU-band group, the predicted communication rate used during iterative selection is

This load-aware rate is an estimate used for ranking. The realized rate is recalculated after all selections using the actual sharing count and sensing-time fraction.

3.3 Monostatic sensing link

The sensing model uses a monostatic radar equation with stochastic class- and band-dependent radar cross section. The processing gains are derived from 1024 and 2048 coherent samples rather than inserted as unexplained constants. The echo SNR is

Dynamic blocker attenuation is applied once on the outward path and once on the return path. The detector uses an exploratory coherent-SNR threshold; it is not a detector-level implementation of the strictest ETSI false-positive or false-negative targets.

3.4 Joint feasibility and equal-denominator goodput

An attempted selection is jointly feasible when its realized direct-link SNR exceeds the communication threshold, its realized echo SNR exceeds the sensing threshold, and the target remains within the 60 m sensing horizon. End-to-end latency and packet reliability are not included in this Boolean event.

The primary goodput metric uses every host-target observation as the denominator:

The paper separately reports selection probability, violation fraction among attempted selections, conditional successful-service rate, and fifth-percentile unconditional goodput. This avoids rewarding a conservative method merely for omitting difficult cases from its rate distribution.

4. DSA-HISAC Selection Heuristic

4.1 Ideal decision objective and implemented approximation

The ideal online problem is to maximize risk-weighted goodput while constraining communication and sensing failures, shared resources, and switching. Solving the full stochastic mixed-integer program at every frame would require joint association, target assignment, and resource allocation. DSA-HISAC instead implements a deterministic approximation: conservative screening, load-aware iterative ranking, post-assignment rate calculation, and hysteresis. No global optimality or exact constraint-preservation claim is made.

4.2 Conservative dual-SNR screening

Estimated communication and sensing SNRs are reduced by a confidence margin ζσ. A candidate remains eligible only when both lower bounds exceed their respective thresholds and the predicted blockage probability remains below a band-specific gate.

$$\gamma^c = \hat{\gamma}^c - \zeta\sigma^c, \quad \gamma^s = \hat{\gamma}^s - \zeta\sigma^s \qquad (6)$$

4.3 Risk- and load-aware utility

Eligible candidates are ranked using normalized communication margin, sensing margin, predicted blockage reliability, service risk, energy cost, and anticipated shared rate. The coefficients are simulation design choices and are disclosed in the configuration. The ranking is repeated until predicted group loads stabilize or the iteration limit is reached.

4.4 Frequency-band hysteresis

A change between 28 and 142 GHz is accepted only when the new utility exceeds the current utility by the hysteresis margin, except when the current link is no longer eligible. The switching metric counts frequency-band changes, not every change of RSU association.

4.5 Risk-adaptive sensing

The sensing scheduler assigns shorter nominal intervals to high-risk targets. Crucially, information age is reset only after the scheduled scan yields at least one valid sensing link. A failed scan leaves age unchanged except for normal accumulation. If target risk rises, an existing long deadline is shortened immediately.

Here uq(t)=1 only when sensing is scheduled and the realized sensing threshold is met. The revised evaluation reports scheduled scans, valid updates, failed-update fraction, mean age, 95th-percentile age, and high-risk age violations.

4.6 Online procedure

1. Predict next-frame object states and construct RSU-object link estimates.
2. For each connected host, retain the single highest-risk target within 60 m.
3. Form 28/142-GHz communication-target candidate pairs for each RSU.
4. Apply method-specific communication, sensing, confidence, and blockage screening.
5. Iterate candidate ranking using anticipated RSU-band sharing load.
6. Apply band hysteresis for DSA-HISAC and record the final selections.
7. Recalculate actual bandwidth sharing, realized rate, sensing overhead, and joint feasibility.
8. Store unconditional goodput, conditional rate, no-selection outcome, violation, switching, and computation time.

5. Experimental Methodology

5.1 Campaign design

The primary campaign uses 30 matched seeds at each of four arrival-demand levels: 300, 600, 900, and 1200 vehicles/hour/approach. Each run contains 60 s of SUMO time with a 10 s warm-up. The controller is evaluated every 100 ms. This frame is a decision-update interval, not evidence that a 20 ms end-to-end service deadline is met.

Demand label	Arrival flow/approach	Mean host-target observations/run	Seeds
Low	300	2601	30
Medium	600	5514	30
High	900	7672	30
Congested	1200	8774	30

5.2 Radio and sensing parameters

The 142 GHz transmit and gain assumptions are not claimed to represent a finalized roadside product. Propagation, hardware, and target-scattering inputs are separated in the parameter-provenance table and varied in the sensitivity analysis. Atmospheric attenuation follows ITU-R P.676 assumptions documented in the configuration.

5.3 Compared methods

5.4 Metrics and statistics

The primary metrics are joint-feasibility fraction and mean unconditional joint-service goodput. Secondary metrics are fifth-percentile unconditional goodput, conditional successful-service rate, no-selection fraction, violation fraction among attempts, sensing time, band switches, and controller computation per evaluated frame. The simplified delivery-delay proxy consists only of a fixed 5 ms processing term plus packet serialization; it is reported in the data package but is not treated as end-to-end latency.

Matched per-seed comparisons use two-sided Wilcoxon signed-rank tests, percentile bootstrap 95% confidence intervals for oriented mean differences, Holm correction, paired Cohen dz, and matched rank-biserial correlation. Effects are reported overall and by traffic-demand level. The experimental unit is a matched run, not each vehicle-time observation.

6. Results

6.1 Joint feasibility

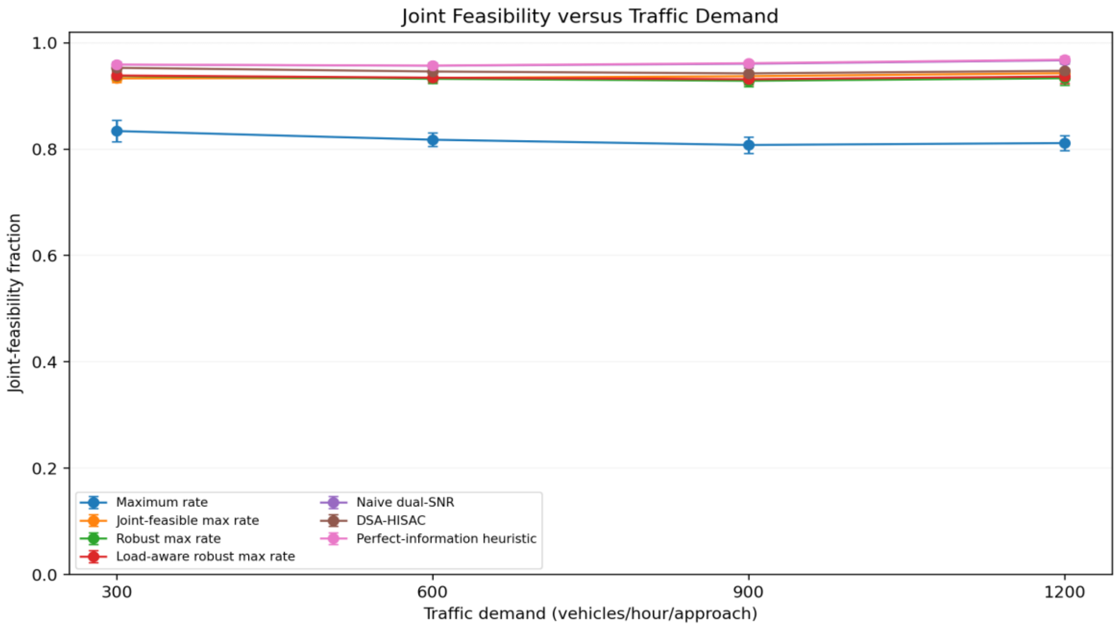

Fig. 3. Joint-feasibility fraction versus traffic demand. Error bars are 95% run-level normal-approximation confidence intervals; paired inferential results use percentile bootstrap intervals and Wilcoxon tests.

Across all 120 runs, DSA-HISAC achieved a joint-feasibility fraction of 0.9467. Maximum-rate selection achieved 0.8173; load-aware robust max-rate achieved 0.9348; naive dual-SNR achieved 0.9604. The strongest comparison is not the communication-only maximum-rate baseline but the load-aware robust maximum-rate method, because both enforce conservative joint-link criteria. DSA-HISAC changes joint feasibility by +1.19 percentage points relative to that baseline.

The matched overall difference versus load-aware robust max-rate was +0.0119, with percentile bootstrap 95% CI [+0.0113, +0.0126], Holm-adjusted Wilcoxon p=1.75e-19, and matched rank-biserial correlation +1.000.

6.2 Equal denominator goodput

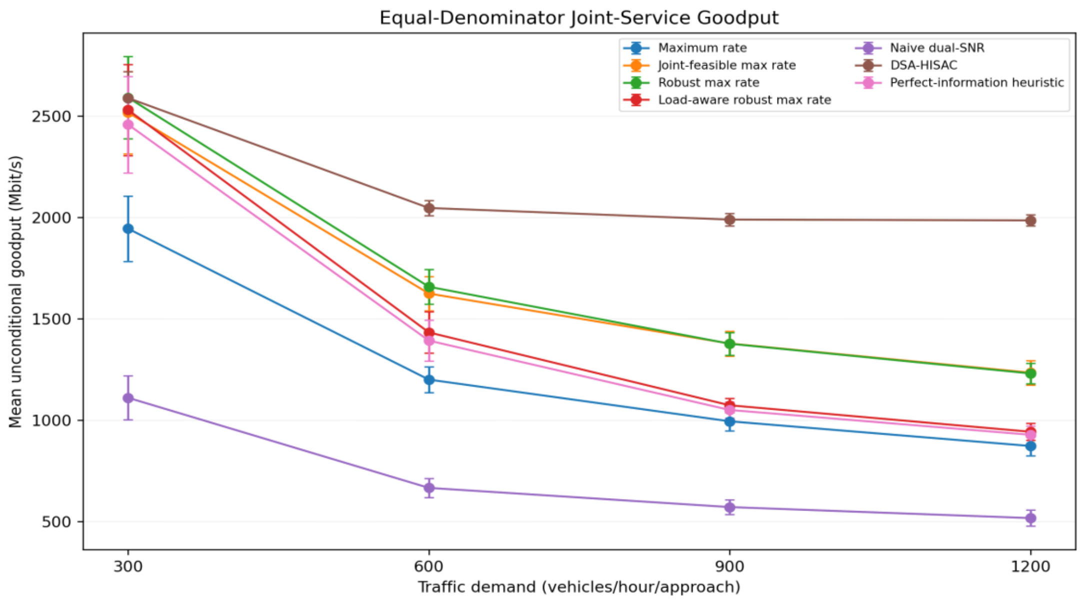

Fig. 4. Mean unconditional goodput. Every host-target observation enters the denominator; no selection and failed joint feasibility contribute zero.

DSA-HISAC produced 2151.8 Mbit/s mean unconditional goodput and 428.5 Mbit/s fifth-percentile unconditional goodput. The corresponding mean goodputs were 1252.2 Mbit/s for maximum-rate selection and 1494.1 Mbit/s for load-aware robust max-rate. Conditional on successful joint service, DSA-HISAC delivered 2272.9 Mbit/s; this conditional quantity is reported separately and is not called overall throughput.

Against load-aware robust max-rate, the oriented mean goodput difference was +657.7 Mbit/s, 95% CI [+573.6, +738.0], Holm-adjusted p=4.97e-17, and rank-biserial correlation +0.923.

6.3 Joint-requirement violations and selection behavior

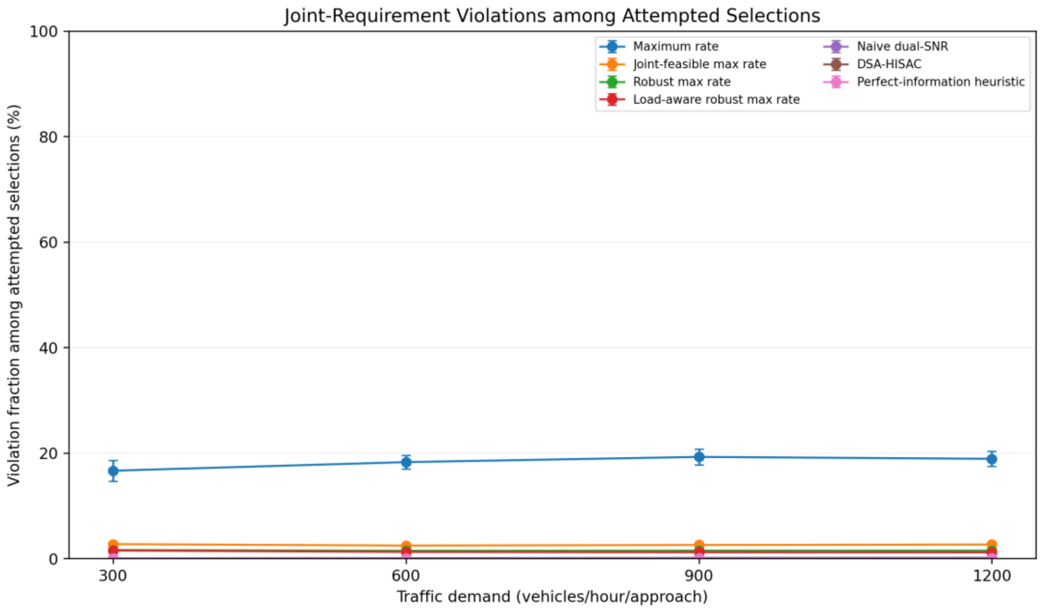

Fig. 5. Fraction of attempted selections that failed at least one realized communication or sensing feasibility requirement. This is not a validated road-safety probability.

The violation fraction among attempted DSA-HISAC selections was 0.022%, compared with 18.27% for maximum-rate selection and 1.283% for load-aware robust max-rate. DSA-HISAC attempted service in 94.69% of host-target observations; the remainder were explicit no-selection outcomes rather than omitted rate samples.

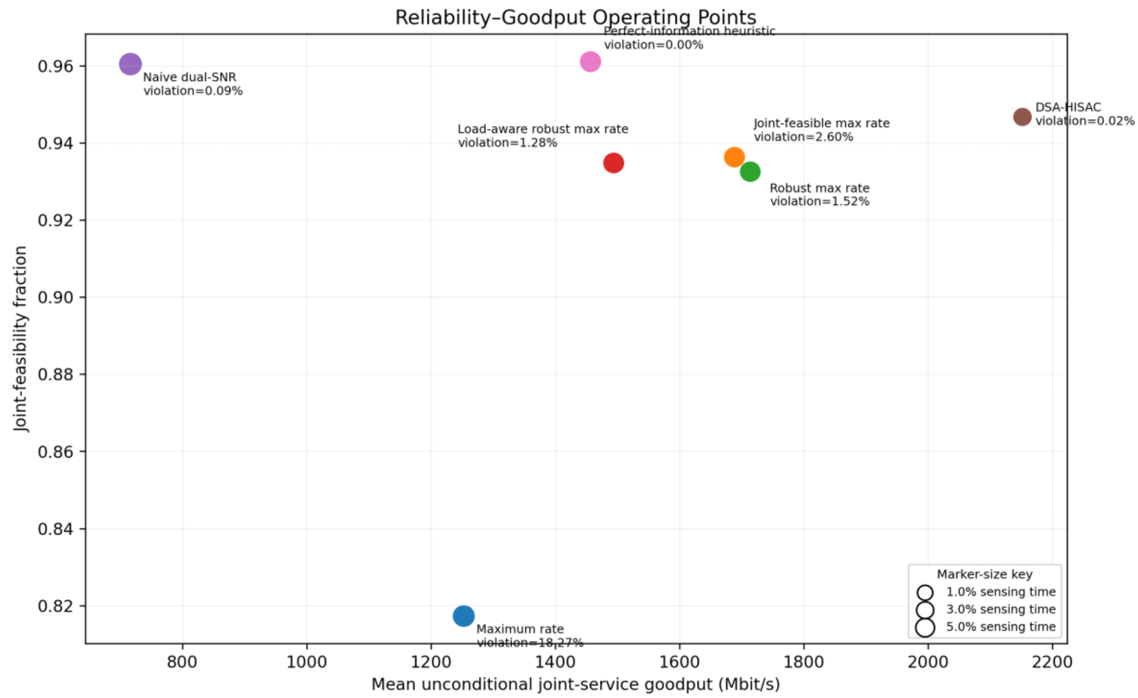

Fig. 6. Reliability-goodput operating points. Marker size represents sensing-time fraction and includes a size legend.

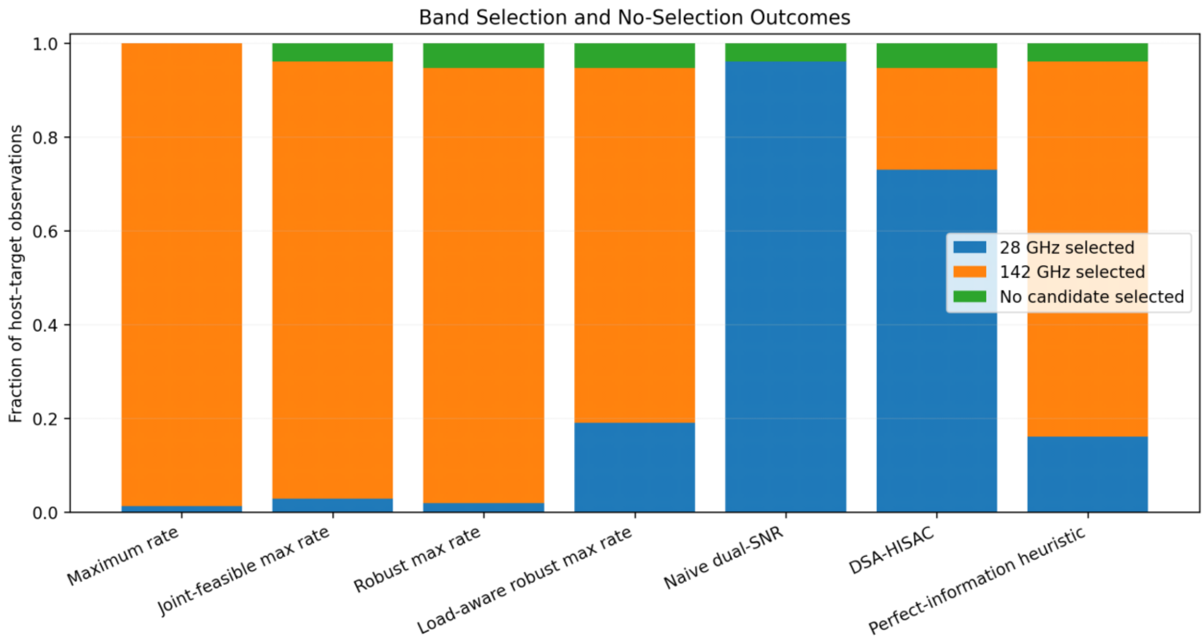

Fig. 7. Fractions assigned to 28 GHz, 142 GHz, or no selected candidate. The caption matches all plotted categories.

6.4 Strong baselines and ablations

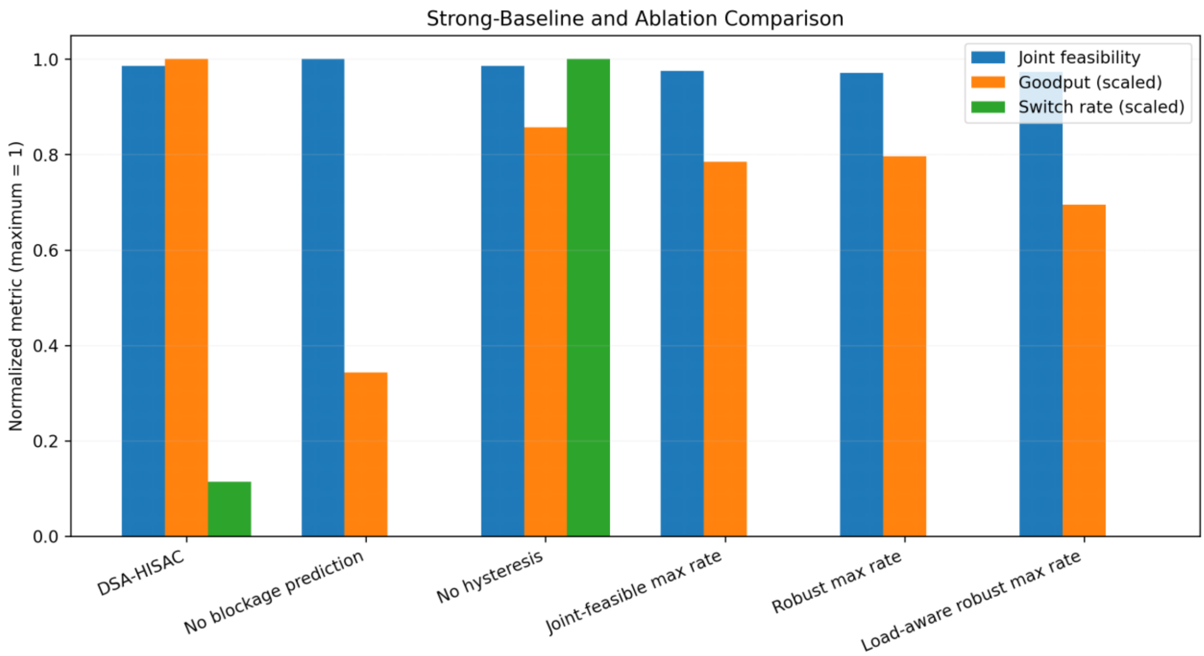

Fig. 8. Normalized comparison of DSA-HISAC, stronger joint-feasible baselines, and ablations. Values are normalized only for visual comparison; the underlying absolute values are reported in Table 3.

Method	Joint feasible	Mean goodput	P5 goodput	Violation/attempt	Band switches/min
Maximum-rate	0.8173	1252.2	0.0	18.268%	0.00
Joint-feasible max-rate	0.9363	1687.8	120.1	2.603%	0.00
Robust max-rate	0.9325	1713.5	137.4	1.521%	0.00
Load-aware robust max-rate	0.9348	1494.1	137.9	1.283%	0.00
Naive dual-SNR	0.9604	715.7	223.1	0.093%	0.00
DSA-HISAC	0.9467	2151.8	428.5	0.022%	189.54
Ablation: no blockage	0.9600	738.7	222.2	0.070%	0.00

Ablation: no hysteresis	0.9467	1844.5	294.9	0.029%	1656.57
Oracle	0.9611	1456.5	341.1	0.000%	0.00

The perfect-information method is a heuristic benchmark rather than a mathematical upper bound because its structure still performs local candidate ranking and post-selection sharing. The no-hysteresis ablation isolates switching stabilization; the no-blockage ablation isolates predicted obstruction. These comparisons prevent the performance argument from relying only on structurally weak communication-centric baselines.

6.5 Risk-adaptive sensing with valid updates

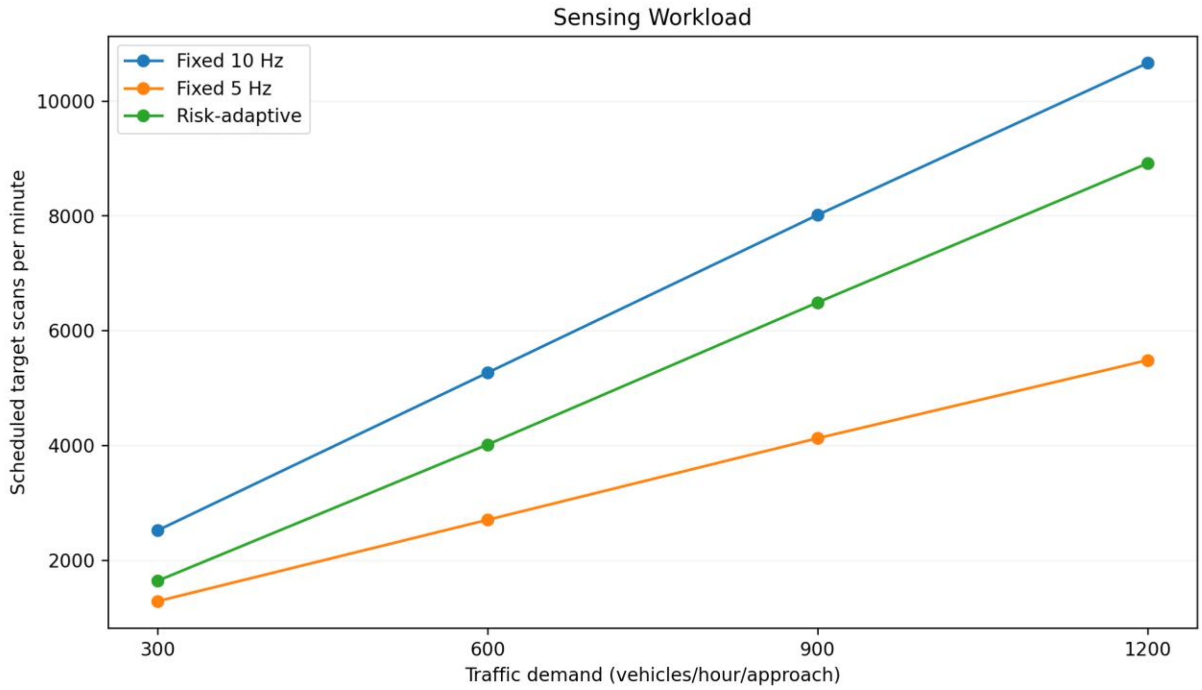

Fig. 9. Scheduled target scans per minute for fixed and risk-adaptive policies.

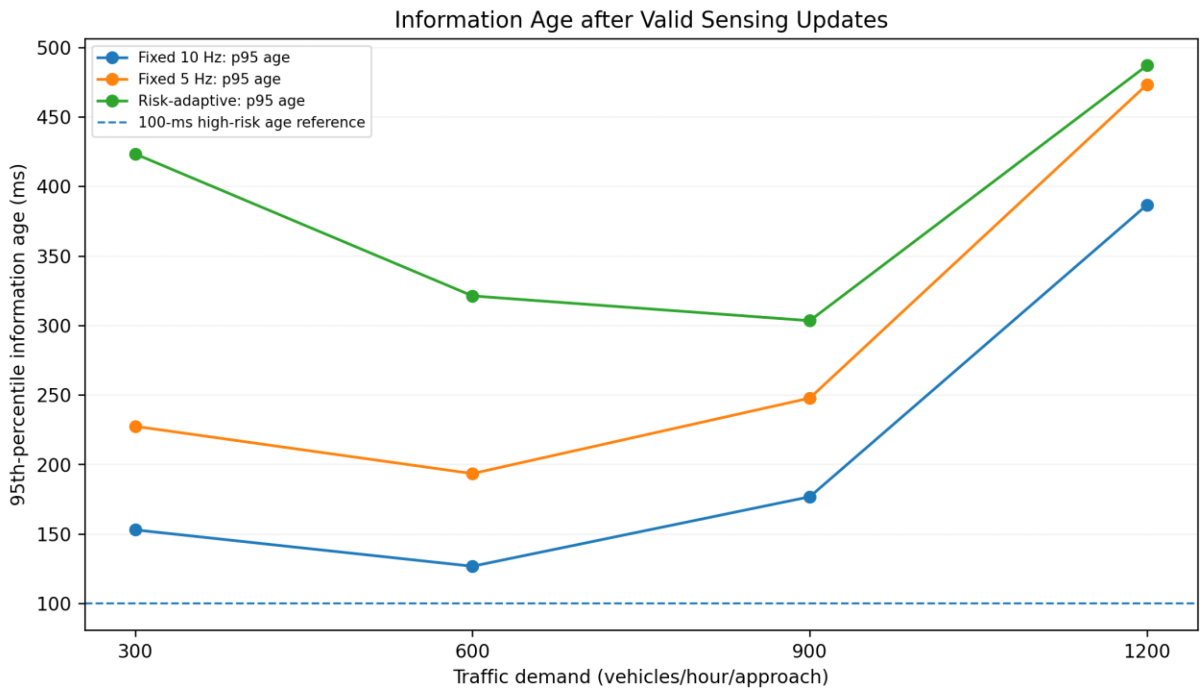

Fig. 10. 95th-percentile information age, reset only after a valid sensing update.

Risk-adaptive scheduling reduced scan demand by 20.4% relative to fixed 10 Hz sensing. Its failed-update fraction was 4.04%, mean age was 89.9 ms, and 95th-percentile age was 383.7 ms. The high-risk age-violation fraction was 2.03%. Unlike the previous draft, a scheduled but invalid sensing attempt does not reset age.

6.6 Runtime and sensitivity

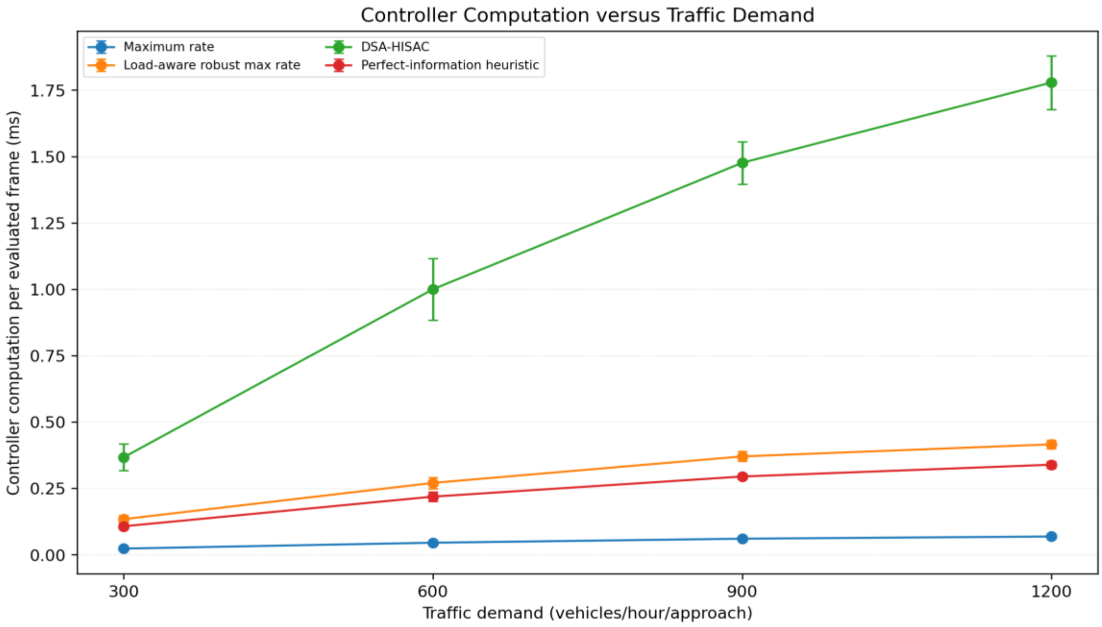

Fig. 11. Controller computation per evaluated frame. The denominator excludes warm-up frames.

Runtime is reported on the recorded software environment in the supplement, including CPU, operating system, Python version, median, 95th percentile, and maximum wall-clock run time. Decision compute time is divided by evaluated frames only. Frequency-band switch counts do not include all RSU association changes.

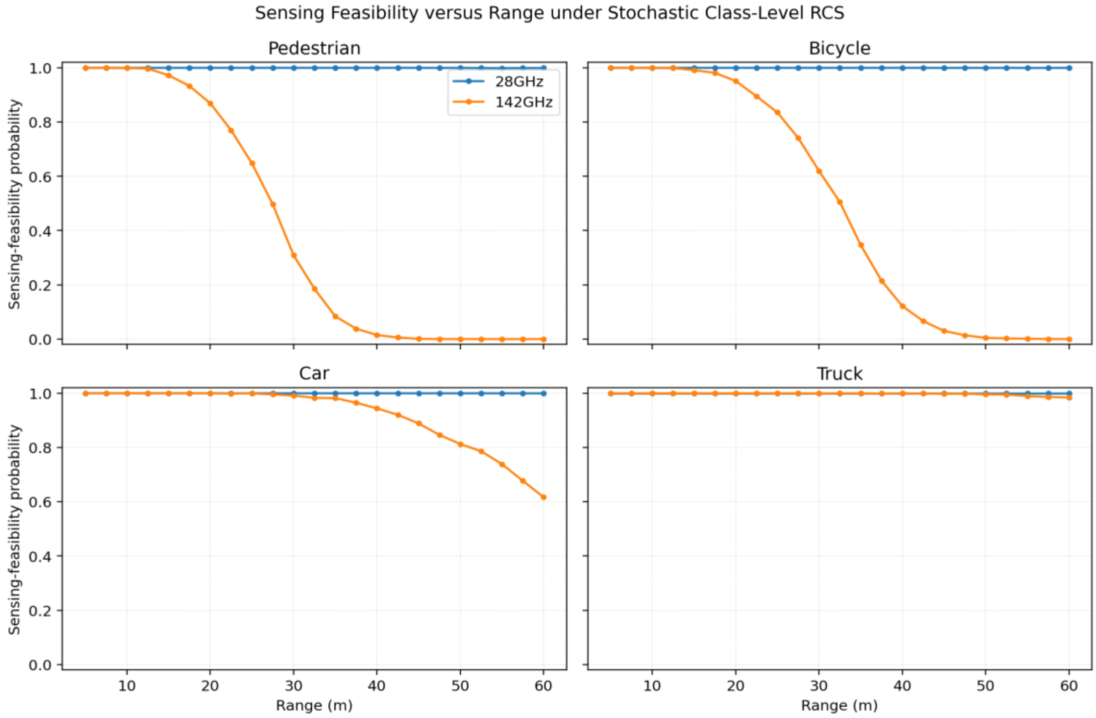

Fig. 12. Monte Carlo sensing-feasibility probability versus range for four target classes. This sensitivity figure is designed to expose dependence on RCS and processing assumptions rather than to validate a specific detector.

The sensitivity study varies processing gain, RCS, sensing threshold, blocker attenuation, transmit power, noise figure, and gas attenuation. It demonstrates that target-echo feasibility is an assumption-sensitive component of the conclusions. The main paper therefore avoids presenting the exploratory 10.34 dB threshold as a standards-compliant detection specification.

7.Discussion

The corrected results support a narrower conclusion than the original draft. DSA-HISAC is useful when the system designer values conservative realized joint feasibility, goodput under an equal denominator, lower violation risk, and stable band use. It is not guaranteed to maximize either availability or conditional rate independently. Naive dual-SNR may accept more opportunities; robust rate baselines may approach or exceed DSA-HISAC on individual metrics; and the preferred operating point depends on application cost.

The principal engineering insight is that direct-link and echo-link quality must be evaluated separately. A wideband 142 GHz communication link may be attractive while the frequency-dependent echo is weak, especially for pedestrians and bicycles. Conversely, a conservative screening margin may reject usable links. The algorithm therefore exposes a controllable conservatism-availability trade-off rather than eliminating it.

The 100 ms controller interval is appropriate for the simulated sensing-cycle study but is not reconciled with a 20 ms end-to-end V2X latency guarantee. Packet coding, retransmission, queueing, beam acquisition, and edge-network delay are absent. The simplified delivery-delay column is retained only as an implementation diagnostic.

8. Limitations and Threats to Validity

Threat	Implication
Simulation scope	One intersection geometry, four RSUs, one highest-priority target per connected host, and 60 s runs.
Radio abstraction	No waveform samples, finite-blocklength packet model, retransmission, adjacent-channel interference, or hardware calibration.
No beam tracker	Fixed antenna gains are used; beamwidth, codebook search, angular uncertainty, and alignment loss are not evaluated.
Sensing detector	Threshold-based coherent-SNR proxy rather than a complete ETSI false-alarm/detection implementation.
Target scattering	Stochastic class- and band-dependent RCS, not geometry-derived aspect-angle scattering for every target.
Algorithmic optimality	Load-aware heuristic; no global mixed-integer optimum and no proof that every estimated constraint remains feasible after sharing.
Perfect-information reference	Heuristic benchmark, not a guaranteed upper bound.
Latency and reliability	No end-to-end latency, packet error, coding, or 99.9% service-reliability validation.
Generalization	Confidence intervals quantify seeded scenario variability, not uncertainty across cities, weather, hardware, or operators.

These limitations bound the claim to comparative performance within the documented simulation. They do not support a claim of deployment readiness, standards compliance, certified road safety, or universal superiority.

9. Security, Privacy, and Deployment Considerations

Roadside sensing can be observed bystanders and non-subscribers. A deployment would require authenticated sensing sources, target provenance, uncertainty representation, retention limits, purpose-based access, and safeguards against ghost-target injection and environmental manipulation. ETSI treats security, privacy, trustworthiness, and sustainability as dedicated ISAC design areas [18]. These functions are architectural requirements but are not evaluated by the present algorithm.

Practical deployment also requires spectrum authorization, coexistence with automotive radar, cross-vendor object formats, calibration, liability rules, and lifecycle energy analysis. The 142 GHz hardware assumptions should be replaced by measured roadside transceiver characteristics before field conclusions are drawn.

Conclusion

This paper presented DSA-HISAC, a conservative load-aware heuristic for hybrid 28/142-GHz roadside ISAC at an urban intersection. After correcting the evaluation to use equal-denominator goodput and stronger joint-feasible baselines, DSA-HISAC achieved joint feasibility 0.9467, mean unconditional goodput 2151.8

Mbit/s, and an attempted-selection violation fraction of 0.022%. Its advantage is not universal: it represents one operating point among availability, goodput, sensing demand, and band switching. The valid-update sensing scheduler reduces scheduled work while explicitly accounting for failed sensing attempts. The next step is waveform-level, hardware-in-the-loop, and outdoor 142 GHz validation with measured blockage, calibration, target RCS, queueing, packet reliability, and multiple simultaneous targets per host.

Data and Reproducibility

The accompanying package includes the revised simulator, SUMO network, fixed configurations, 120 run-level campaign records, aggregate data, paired statistical tests, parameter sensitivity, figures, manuscript source, and validation files. All main figures are generated from stored outputs. The package reproduces the simulation findings but is not a substitute for independent experimental validation.

Reference

1. F. Liu, C. Masouros, A. P. Petropulu, H. Griffiths, and L. Hanzo, 'Joint radar and communication design: Applications, state-of-the-art, and the road ahead,' IEEE Trans. Commun., vol. 68, no. 6, pp. 3834–3862, 2020, doi: 10.1109/TCOMM.2020.2973976.
2. J. A. Zhang et al., 'An overview of signal processing techniques for joint communication and radar sensing,' IEEE J. Sel. Topics Signal Process., vol. 15, no. 6, pp. 1295–1315, 2021, doi: 10.1109/JSTSP.2021.3113120.
3. F. Liu et al., 'Integrated sensing and communications: Toward dual-functional wireless networks for 6G and beyond,' IEEE J. Sel. Areas Commun., vol. 40, no. 6, pp. 1728–1767, 2022, doi: 10.1109/JSAC.2022.3156632.
4. F. Liu, W. Yuan, C. Masouros, and J. Yuan, 'Radar-assisted predictive beamforming for vehicular links: Communication served by sensing,' IEEE Trans. Wireless Commun., vol. 19, no. 11, pp. 7704–7719, 2020, doi: 10.1109/TWC.2020.3015735.
5. W. Yuan, F. Liu, C. Masouros, J. Yuan, D. W. K. Ng, and N. Gonzalez-Prelcic, 'Bayesian predictive beamforming for vehicular networks: A low-overhead joint radar-communication approach,' IEEE Trans. Wireless Commun., vol. 20, no. 3, pp. 1442–1456, 2021, doi: 10.1109/TWC.2020.3033776.
6. C. Liu et al., 'Learning-based predictive beamforming for integrated sensing and communication in vehicular networks,' IEEE J. Sel. Areas Commun., vol. 40, no. 8, pp. 2317–2334, 2022, doi: 10.1109/JSAC.2022.3180803.
7. X. Meng, F. Liu, C. Masouros, W. Yuan, Q. Zhang, and Z. Feng, 'Vehicular connectivity on complex trajectories: Roadway-geometry aware ISAC beam-tracking,' IEEE Trans. Wireless Commun., vol. 22, no. 11, pp. 7408–7423, 2023, doi: 10.1109/TWC.2023.3250442.
8. Z. Du et al., 'Integrated sensing and communications for V2I networks: Dynamic predictive beamforming for extended vehicle targets,' IEEE Trans. Wireless Commun., vol. 22, no. 6, pp. 3612–3627, 2023, doi: 10.1109/TWC.2022.3219890.
9. A. M. Elbir et al., 'Terahertz-band integrated sensing and communications: Challenges and opportunities,' IEEE Aerosp. Electron. Syst. Mag., vol. 39, no. 12, pp. 38–49, 2024, doi: 10.1109/MAES.2024.3476228.
10. D. Shakya et al., 'Radio propagation measurements and statistical channel models for outdoor urban microcells in open squares and streets at 142, 73, and 28 GHz,' IEEE Trans. Antennas Propag., 2024, doi: 10.1109/TAP.2024.3366581.
11. Y. Xing and T. S. Rappaport, 'Millimeter wave and terahertz urban microcell propagation measurements and models,' IEEE Commun. Lett., vol. 25, no. 12, pp. 3755–3759, 2021, doi: 10.1109/LCOMM.2021.3117900.
12. N. A. Abbasi et al., 'Measurement of directionally resolved radar cross section of human body for 140 and 220 GHz bands,' in Proc. IEEE WCNC Workshops, 2020, doi: 10.1109/WCNCW48565.2020.9124817.
13. Q. Zhang et al., 'Design and performance evaluation of joint sensing and communication integrated system for 5G mmWave enabled connected and automated vehicles,' arXiv:2108.10535, 2021.
14. H. Liu, Z. Wei, X. Li, Y. Geng, Q. Zhang, and Z. Feng, 'Beyond single-band: Analysis and resource allocation for multi-band ISAC systems,' arXiv:2607.08068, July 2026.
15. 3GPP, 'Study on channel model for frequencies from 0.5 to 100 GHz,' TR 38.901 V18.0.0, May 2024.
16. ETSI, 'Integrated sensing and communications: Use cases and deployment scenarios,' ETSI GR ISC 001 V1.1.1, Mar. 2025.
17. 5G Automotive Association, 'Study on integrated sensing and communication for C-V2X application,' Technical Report V1.0, May 2025.
18. ETSI, 'Integrated sensing and communications: Security, privacy, trustworthiness and sustainability,' ETSI GR ISC 004 V1.1.1, Feb. 2026.
19. ETSI, 'Integrated sensing and communications: Channel modelling, measurements and evaluation methodology,' ETSI GR ISC 002 V1.1.1, Aug. 2025.
20. ITU-R, 'Attenuation by atmospheric gases and related effects,' Recommendation ITU-R P.676-13, 2022.
21. P. A. Lopez et al., 'Microscopic traffic simulation using SUMO,' in Proc. IEEE ITSC, pp. 2575–2582, 2018, doi: 10.1109/ITSC.2018.8569938.
22. P. Kumari, J. Choi, N. Gonzalez-Prelcic, and R. W. Heath Jr., 'IEEE 802.11ad-based radar: An approach to joint vehicular communication-radar system,' IEEE Trans. Veh. Technol., vol. 67, no. 4, pp. 3012–3027, 2018, doi: 10.1109/TVT.2017.2774762.